Water Air Soil Pollut (2020) 231: 425
https://doi.org/10.1007/s11270-020-04768-8

Different Iron Oxalate Sources as Catalysts on Pyrazinamide Degradation by the Photo-Fenton Process at Different pH Values

Ivan I. Conde-Morales · Laura Hinojosa-Reyes · Jorge L. Guzmán-Mar · Aracely Hernández-Ramírez · Isabel del Carmen Sáenz-Tavera · Minerva Villanueva-Rodríguez

Received: 23 March 2020 / Accepted: 13 July 2020 / Published online: 2 August 2020

Abstract The presence of emerging contaminants (EC), such as antibiotics in water bodies, is considered an environmental issue. In this work, the iron sources FeC_2O_4•$2H_2O$ (FOD), complexes of iron/oxalate (Fe^{2+}/Ox), and $FeSO_4$ as reference were evaluated as catalysts on the degradation of pyrazinamide (10 mg L^{-1}) antibiotic by the photo-Fenton process. Different parameters were studied such as initial pH value (3, 4.5, and 6), Fe^{2+}/H_2O_2 molar ratio (1:20, 1:30, and 1:40), and Fe^{2+}/Ox with different molar ratios (1:3, 1:6, and 1:9). The best performance was achieved with a 1:20 Fe^{2+}/H_2O_2 molar ratio using $FeSO_4$ and FOD showing similar results as $FeSO_4$ catalyst at pH 3 and 4.5. The degradation rate at pH 6 was enhanced using Fe^{2+}/Ox (1:3) compared to $FeSO_4$, and this behavior was explained by Fenton reactants consumption and the oxalate use. The iron source FOD exhibited a poor performance at pH 6 compared with $FeSO_4$; however, FOD activity was notably increased at pH 6 using a greater amount of catalyst, reaching 86.8% of pyrazinamide degradation in 60 min, even higher than using Fe^{2+}/Ox 1:3 complex (68.9%), which makes it a suitable catalyst for the degradation of pyrazinamide by the photo-Fenton process.

I. I. Conde-Morales · L. Hinojosa-Reyes · J. L. Guzmán-Mar · A. Hernández-Ramírez · I. d. Sáenz-Tavera · M. Villanueva-Rodríguez (✉)
Universidad Autonoma de Nuevo Leon, UANL, Facultad de Ciencias Quimicas, Ave. Universidad s/n, Ciudad Universitaria, 66455 San Nicolás de los Garza, Nuevo León, Mexico
e-mail: minerva.villanuevardr@uanl.edu.mx

Keywords Degradation · Emerging contaminant · Humboldtine · Oxalate · Photo-Fenton process · Pyrazinamide

1 Introduction

In recent years, emerging contaminants (EC) have been detected in wastewater, surface, and groundwater bodies (Taheran et al. 2018). Those EC represent a risk for human health and the environment. Pharmaceutical products are considered as EC that could be released to the environment by the pharmaceutical industry, hospital discharges, and effluents from wastewater treatment plants (WWTP) (Tran et al. 2018). The presence of antibiotics in the aquatic environment is a concern since they can cause bacterial resistance, and these compounds are well known for being difficult to be treated by conventional methods in WWTP (Luo et al. 2014; Tran et al. 2018). The presence of antituberculosis drugs, a class of antibiotics, has been scarcely studied in the environment; however, they are widely prescribed in Latin America and African countries where tuberculosis disease is still prevalent (Muñoz del Carpio-Toia et al. 2018). Pyrazinamide (PYR) is one of the most used antituberculosis drugs. It is reported that 34% of this molecule is excreted from the body without change. It has been estimated the release of 19,856 kg/year of PYR to the environment (Magwira et al. 2019) in countries like South Africa. The predicted environmental concentration of 7.5 μg L^{-1} for PYR has been estimated in countries like China with a risk quotient

lower than 1 (Chen et al. 2015); however, being an antibiotic this molecule and its active moiety, the pyrazinoic acid could induce bacterial resistance even at low concentration. Therefore, the evaluation of alternative remediation strategies for removal of this kind of drug is required for cleaning the water ecosystem.

The Fenton reaction-based processes and the heterogeneous photocatalysis are promising alternatives to remove the EC, and both treatments belong to the advanced oxidation technologies (AOTs). In the Fenton reaction, the homolytic break of H_2O_2 by Fe^{2+} (Eq. 1) occurs to generate HO• ($E^0 = 2.80$ V vs. NHE) and the formation of the corresponding Fe^{3+} hydroxo-complexes (Eq. 2). This treatment could be improved by applying UV radiation, namely photo-Fenton, where Fe^{3+} is photo-reduced leading to the hydroxyl radicals production from the ferric hydroxo-complexes (Eq. 3), and also the UV radiation allows photo-decomposition of formed ferric-carboxylate complexes (Pouran et al. 2015). Additionally, H_2O_2 ($E^0 = 1.78$ V vs. NHE) can be photolyzed, enhancing HO• production (Eq. 4).

$$Fe^{2+} + H_2O_2 \rightarrow Fe^{3+} + OH^- + HO^{\bullet} \quad (1)$$

$$Fe^{3+} + OH^- \rightarrow Fe(OH)^{2+} \quad (2)$$

$$Fe(OH)^{2+} + h\nu \rightarrow Fe^{2+} + HO^{\bullet} \quad (3)$$

$$H_2O_2 + h\nu \rightarrow 2\ HO^{\bullet} \quad (4)$$

The Fe^{2+}/H_2O_2 molar ratio is one of the main factors that influence the Fenton treatment efficiency since these reactants could also act as HO• scavengers at elevated concentrations (Eqs. 5 and 6) (Pouran et al. 2015).

$$H_2O_2 + HO^{\bullet} \rightarrow H_2O + HO_2^{\bullet} \quad (5)$$

$$Fe^{2+} + HO^{\bullet} \rightarrow Fe^{3+} + HO^- \quad (6)$$

The photo-Fenton process has been applied for degrading several organic contaminants showing the highest efficiency in acidic medium (pH 2.8–3.0) (Pouran et al. 2015). One strategy to enhance photo-Fenton degradation capability and to prevent iron precipitation at pH > 3 is the use of organic iron complexes that increase its solubility and photosensitivity (Nogueira et al. 2017; Expósito et al. 2018). Several ligands (e.g., oxalate, citrate, formate, maleate, EDTA) have been studied, obtaining better results with oxalate at pH 2.8 (Kwan and Chu 2007; Manenti et al. 2015; Soares et al. 2015), at near pH 5.0 (Lee et al. 2014; Souza et al. 2014; Nogueira et al. 2017; Expósito et al. 2018), and close to neutrality (pH 6) (Villegas-Guzman et al. 2017). The positive effect of Fe-oxalate complexes has been attributed to its facile photo-decarboxylation and Fe^{2+} regeneration (Eqs. 7 and 8) (Souza et al. 2014; Clarizia et al. 2017).

$$Fe(C_2O_4)_3^{3-} + h\nu \rightarrow Fe^{2+} + 2C_2O_4^{2-} + C_2O_4^{\bullet-} \quad (7)$$

$$C_2O_4^{\bullet-} + O_2 \rightarrow 2\ CO_2 + O_2^{\bullet-} \quad (8)$$

The Fe^{2+}/Ox complexes prepared in situ have demonstrated to be more efficient than the ferrous (Monteagudo et al. 2013; Seiberta et al. 2017) or ferric salts (De Lima Perini et al. 2013; Conte et al. 2016) as an iron source. In this system, the Fe^{2+}/Ox molar ratio is a substantial contributing factor. The Fe^{2+}/Ox molar ratio 1:3 is commonly used, due to the formation of a stable iron oxalate complex (Monteagudo et al. 2013; Manenti et al. 2015; Pouran et al. 2015); nevertheless, elevated molar ratios (e.g., 1:9, 1:10, and 1:20) have also shown good results (De Luca et al. 2014; Souza et al. 2014; Conte et al. 2016).

On the other hand, in recent years, ferrous oxalate dihydrate ($FeC_2O_4 \cdot 2H_2O$, humboldtine) has been studied as a promising and stable semiconductor for its application in the degradation of dyes as Rhodamine B and methylene blue or decomposition of aniline by heterogeneous photocatalysis (Fan et al. 2016; Liu et al. 2016); also, it has been studied as a possible iron source in the photo-Fenton reaction (Liu et al. 2017; Hu et al. 2019; Wang et al. 2019).

In the present work, the antituberculosis drug PYR, a recalcitrant molecule, was used as a model water pollutant to compare the efficiency of the photo-Fenton process using different ferrous sources. The degradation of PYR by advanced oxidation technologies has been scarcely described mainly based on heterogeneous photocatalysis (Guevara-Almaraz et al. 2015; Jo and Natarajan 2015; Stets et al. 2018) and electro-Fenton (Arhoutane et al. 2019). Thus, this work aimed to evaluate the performance of the photo-Fenton process using

FOD and Fe^{2+}/Ox complexes as iron sources to degrade PYR at different pH values (3, 4.5, and 6) comparing with conventional Fenton reaction using $FeSO_4$.

2 Materials and Methods

2.1 Reagents

All chemicals utilized were reagent grade and used as received. Pyrazinamide (pyrazine carboxamide 99%), ferrous oxalate dihydrate (FeC_2O_4•$2H_2O$, 99%), sodium 1-heptanesulfonate, and titanium oxysulfate (99%) were from Sigma-Aldrich. Ferrous sulfate ($FeSO_4$•$7H_2O$, 99%) was purchased from Jalmek. Hydrogen peroxide (H_2O_2, 30%), sodium hydroxide (NaOH), hydrochloric acid (HCl), sodium oxalate ($Na_2C_2O_4$), 1,10-phenanthroline, and sodium thiocyanate (NaSCN) were supplied from CTR Scientific. Acetonitrile (HPLC grade) from Tedia, acetic acid (HPLC grade) from J.T. Baker, and deionized water from MilliQ water purification system (18.2 MΩ cm resistivity) were used for HPLC analysis.

2.2 Degradation Assays

Batch experiments were carried out using 250 mL of 10 mg L^{-1} PYR solution. The solution pH was adjusted to 3.0, 4.5, and 6.0 with 0.1 M NaOH or 0.1 M HCl; then 0.1 mmol L^{-1} of $FeSO_4$ or FOD and the required amount of H_2O_2 (2–4 mmol L^{-1}) to obtain 1:20, 1:30, or 1:40 Fe^{2+}/H_2O_2 molar ratios were added. Concentrations of Fe^{2+} and H_2O_2 were chosen based on some literature references (Alalm et al. 2015; Expósito et al. 2018; Arhoutane et al. 2019; Seiberta et al. 2017).

The solution mixture was irradiated with a UV lamp (Spectroline model XX-15N, $\lambda = 365$ nm, and an average light intensity of 17 W m^{-2}). The effect of Fe^{2+}/Ox molar ratio was evaluated by preparing the complexes in situ as described elsewhere (Expósito et al. 2018) using specific amounts of $FeSO_4$•$7H_2O$ and $Na_2C_2O_4$ to obtain Fe^{2+}/Ox in 1:3, 1:6, and 1:9 molar ratios; after that, the pH was adjusted (3, 4.5, or 6), and H_2O_2 was added (Fe^{2+}/H_2O_2 molar ratio 1:20). The photocatalytic activity of FOD at pH 6 was also determined with different catalyst loadings (from 0.1 to 7.7 mmol L^{-1}) in the absence or the presence of H_2O_2 (2 mmol L^{-1} H_2O_2). As control tests, photolysis under UV radiation, H_2O_2/UV, and Fenton (i.e., $FeSO_4/H_2O_2$, FOD/H_2O_2, and Fe^{2+}/Ox1:3/H_2O_2) were carried out at pH 3 and Fe^{2+}/H_2O_2 1:20 molar ratio.

2.3 Analytical Methods

FeC_2O_4•$2H_2O$ was characterized by X-ray diffraction (XRD) on a Siemens D5000 diffractometer in the 2θ range from 5 to 90° with a step size of 0.05° to identify the crystalline phase. The semiconductor material was analyzed in a Nicolet, Evolution 300 PC UV-Vis spectrophotometer equipped with a Praying Mantis diffuse reflectance integration sphere to determine the bandgap (Eg) of the catalyst. The Eg value was estimated by extrapolation of the linear part of the plot $[F(R) \times h\upsilon]^n$ vs. energy ($h\upsilon$) according to Kubelka-Munk function, where R is the reflectance, $F(R)$ is proportional to the extinction coefficient (α), and $n = 2$. Raman spectra were recorded in a Thermo Scientific DXR Raman microscope with a laser diode (780 nm) as a radiation source.

During degradation assays, sample aliquots were collected and filtered using 0.45-μm filters (Phenex-RC) and analyzed by liquid chromatography (HPLC, Perkin Elmer Series200) equipped with a UV detector at 270 nm. Chromatographic conditions were adapted from Guevara-Almaraz et al. (2015) using a C-18 ONIX monolithic column (25 × 4.6 mm), and 10 mmol L^{-1} sodium 1-heptanesulfonate (pH 3):acetonitrile (98:2 v/v) as mobile phase at 0.8 mL min^{-1} flow rate and 20 μL injection volume. The limits of detection and quantification were 0.09 mg L^{-1} and 0.36 mg L^{-1}, respectively.

Mineralization of the PYR molecule was monitored by measuring total organic carbon (TOC) content in the aqueous solution with a TOC analyzer (Shimadzu model TOC-VCSH).

During PYR decomposition, Fe^{2+}, H_2O_2, and Fe^{3+} evolution were followed by UV-Vis spectroscopy. Quantification was based on the formation of the colored complexes between Fe^{2+}, Fe^{3+}, and H_2O_2 with 1,10-phenanthroline ($\lambda = 510$ nm), potassium thiocyanate ($\lambda = 450$ nm) (Pehkonen 1995), and titanium oxysulfate ($\lambda = 408$ nm) (Eisenberg 1943), respectively.

3 Results and Discussion

3.1 pH and Fe^{2+}/H_2O_2 Molar Ratio Effect

PYR was effectively eliminated from the solution by the photo-Fenton process. Comparable results were

obtained with $FeSO_4$ and FOD at pH 3, achieving more than 94% of degradation in 60 min using Fe^{2+}/H_2O_2 1:20 and 1:30 (Fig. 1a), and more than 83% at the same time at pH 4.5 with Fe^{2+}/H_2O_2 1:20 (Fig. 1b). However, as the concentration of H_2O_2 increased up to Fe^{2+}/H_2O_2 1:40 ratio, lower degradation efficiency was observed. This effect was attributed to an excess of H_2O_2 in the medium, which acts as $HO^{\bullet}$ scavenger (Eq. 5). Thus, the 1:20 Fe^{2+}/H_2O_2 molar ratio was used in subsequent experiments. The negative effect was more evident, especially at pH 6 using FOD as the iron source. The photolysis of $C_2O_4^{2-}$ produces $C_2O_4^{\bullet-}$ radical, which is then decomposed in CO_2 and $CO_2^{\bullet-}$ ($E^0 = -1.8$ V vs. NHE) (Eq. 9). After, $CO_2^{\bullet-}$ favors O_2 reduction to $O_2^{\bullet-}$ in aerated conditions (Eq. 8) and then, the subsequent formation of H_2O_2 is attained (Jeong and Yoon 2004; Lee et al. 2014; Souza et al. 2014; Chen et al. 2020). Thus, inhibition of the degradation could be caused by a high concentration of H_2O_2 in the bulk solution promoted by the oxalate presence (Jeong and Yoon. 2004; Chen et al. 2020). Besides, FOD could act as a photocatalyst, and the electrons photo-induced at the conduction band could reduce the available oxygen in the medium to produce hydrogen peroxide (Eq. 10) (Fan et al. 2016).

$$C_2O_4^{\bullet-} \rightarrow CO_2 + CO_2^{\bullet-} \quad (9)$$

$$O_2 + 2\,e^- + 2H^+ \rightarrow H_2O_2 \quad (10)$$

Otherwise, an expected lower degradation percentage of PYR was observed at pH 6 (Fig. 1c) than that in acidic medium. Also, the Fe^{2+}/H_2O_2 molar ratio showed a minimum effect on degradation independently of the iron source at this pH value, attributed to the slow decomposition of H_2O_2 at pH 6 (Alalm et al. 2015). It has been reported that at pH 6, the soluble $Fe(OH)_2^+$ complex could be generated, which is less photoactive than the $Fe(OH)^{2+}$ complex (Eq. 2) to regenerate Fe^{2+} reducing the degradation rate (Pereira et al. 2014; Nogueira et al. 2017). Nevertheless, almost complete degradation was achieved after 180 min by conventional photo-Fenton ($FeSO_4$), similar to that reported by Alalm et al. (2015) in the degradation of different pharmaceutical compounds at near-neutral pH.

A remarkable negative effect on PYR degradation efficiency occurred using FOD at pH 6 which can be attributed to a limited amount of available Fe^{2+} in the bulk solution as the solution pH increases, allowing a stronger interaction between Fe and oxalate and disfavoring the reaction with H_2O_2 to produce $HO^{\bullet}$. The release of oxalate from FOD in acidic media has been previously observed (Liu et al. 2019). On the other hand, it is the expected that carboxylated ligands promote the solubility of iron at near-neutral pH; however, the solubility product constant (Ksp) reported for FOD is low, between 2.09×10^{-7} and 3.20×10^{-7} (Jung and Baek 2019; Liu et al. 2019), which could influence Fe^{2+} availability at pH 6 even using a low concentration of Fe^{2+}as in this study (0.1 mmol L^{-1}). Also, a decrease of $HO^{\bullet}$ production at pH 6 has been reported by Li et al. (2018) using electron paramagnetic resonance (EPR) experiments, and the optimal catalytic performance of FOD to produce $HO^{\bullet}$ was allowed at pH 4, which also explains the behavior observed in Fig. 1b and c.

The rate constants for the first stage of the Fenton reaction were estimated using the equation $ln(C_o/C) = k_{app}t$, where k_{app} is the apparent first-order rate constant and C_0 and C are the contaminant concentrations at initial and t time, respectively. The half-life time ($t_{½}$) was calculated from $t_{½} = ln2/k_{app}$. A summary of degradation and kinetic parameters are shown in Table 1. Correlation coefficients (R^2) were > 0.9406 fitting well with pseudo-first-order model.

Similar k_{app} values were obtained using $FeSO_4$ and FOD at pH 3 and 4.5. Nevertheless, at pH 6, $FeSO_4$ attained degradation rate (1.61×10^{-2} min^{-1}) more than sevenfold higher than FOD (0.21×10^{-2} min^{-1}) which reveals a marked difference in iron availability.

3.2 $FeC_2O_4 \cdot 2H_2O$ as Catalyst

The potential activity of FOD as a catalyst was evaluated at pH 6. First, the solid was characterized by XRD and UV-Vis diffuse reflectance spectroscopy (DRS). The crystalline structure of FOD has been described as a distorted octahedral MO_6 arrangement (D'Antonio et al. 2009; Fan et al. 2016). According to Fig. 2, the sample corresponds to the β-crystalline phase Humboldtine (JCPDS 00-023-0293), and the band gap energy calculated from Kubelka-Munk function (insert in Fig. 2) is 1.9 eV which is lower than that reported for the synthesized ferrous oxalate (2.36–2.41 eV) (Liu et al. 2016). In the present work, to better understand the photocatalytic activity of FOD, some tests were conducted in the absence of H_2O_2. The catalyst loading

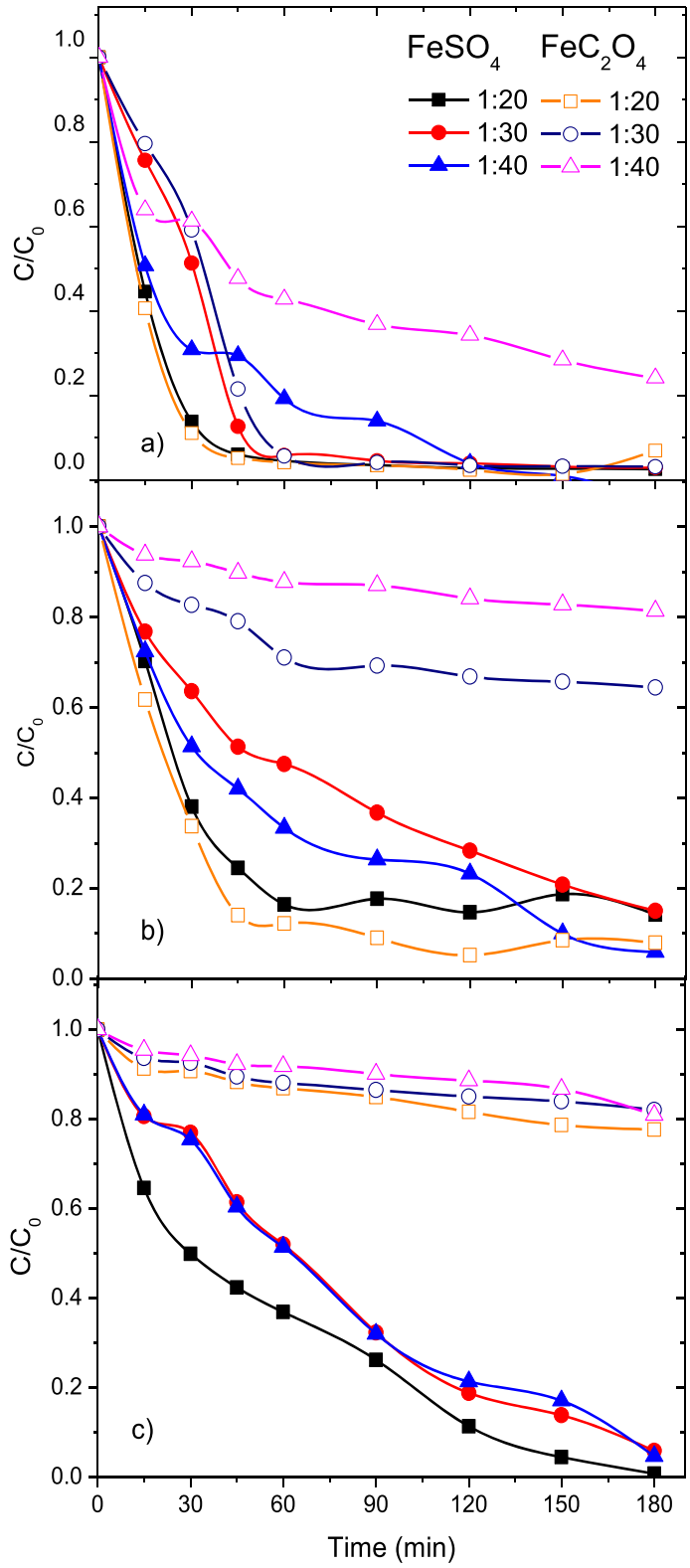

Fig. 1 Graphs were plotted using Origin Pro 8 software. Pyrazinamide degradation at (a) pH 3, (b) pH 4.5, and (c) pH 6 by the photo-Fenton process, using $FeSO_4$ (filled symbols) and FOD (empty symbols) in different molar ratios Fe^{2+}/H_2O_2, (■, □) 1:20, (●, ○) 1:30, and (▲, Δ) 1:40

Table 1 Degradation percentage, kinetic constant, and $t_{1/2}$ for PYR degradation by the photo-Fenton treatment using different iron sources and different pH values

Iron source[a]	pH	% Degradation in 60 min	k_{app} (min^{-1})	R^2	$t_{1/2}$ (min^{-1})
$FeSO_4$	3	95.5	5.46×10^{-2}	0.9686	12.7
	4.5	83.6	3.11×10^{-2}	0.9936	22.3
	6	63.0	1.61×10^{-2}	0.9406	43.1
$FeC_2O_4 \cdot 2H_2O$	3	95.9	5.63×10^{-2}	0.9531	12.3
	4.5	87.7	3.79×10^{-2}	0.9682	18.3
	6	7.2	0.21×10^{-2}	0.9942	330.1
	6[b]	86.8	4.26×10^{-2}	0.9564	16.3
Fe^{2+}/Ox (1:3)	3	99.9	42.67×10^{-2}	0.9831	1.63
	4.5	78.6	13.07×10^{-2}	0.9408	5.30
	6	68.9	9.36×10^{-2}	0.9412	7.40

[a] In all cases $[Fe^{2+}] = 0.1$ mmo L^{-1}, $[H_2O_2] = 2$ mmol L^{-1}, except for [b] [FOD] = 0.2 g L^{-1} (1.1 mmo L^{-1} Fe^{2+})

amounts from 0.2 to 1.4 g L^{-1} FOD were tested (i.e., 1.1 to 7.7 mmol L^{-1} Fe^{2+}).

As shown in Fig. 3, the best result of PYR degradation (35.8%) in the absence of hydrogen peroxide was accomplished in 180 min using 0.2 g L^{-1} of FOD loading. In this condition, higher degradation was obtained than that applying conventional photo-Fenton at pH 6 (23.5%) in the same reaction time (Fig. 1c). This result confirmed that FOD is suitable for use as photocatalyst as was previously described (Fan et al. 2016; Liu et al. 2016). However, the increase of the catalyst loading beyond 0.6 g L^{-1}, caused inhibition of the catalytic activity due to the screening effect (Wang et al. 2019). Therefore, 0.2 g L^{-1} of FOD was selected for PYR degradation at pH 6 in the presence of H_2O_2 (2 mmol L^{-1}). It is worth mentioning that the process using FOD (0.2 g L^{-1}) as the iron source would be considered as a heterogeneous photo-Fenton treatment due to the low solubility of FOD. However, a noticeable enhancement of the degradation percentage was observed under these conditions (Fig. 3). The degradation rate by the photo-Fenton treatment using FOD was higher (4.26×10^{-2} min^{-1}) than that reached with $FeSO_4$ ($1.61 \times 10_{-2}$ min^{-1}) but lower than that using Fe:Ox 1:3 at pH 6 (9.36×10^{-2} min^{-1}) (Table 1). High degradation efficiencies at pH 6 were reported for rhodamine B and methyl orange using 0.2 g L^{-1} of FOD (Li et al. 2018) and for methyl orange using 1 g L^{-1} of Fe/Ni-oxalate by heterogeneous Fenton reaction (Liu et al. 2017). In this work, the results on PYR degradation corroborated that FOD at pH 6 is a promising iron source in the Fenton reaction-based process.

The stability of the synthesized FOD during the degradation of dyes by the photo-Fenton process has been previously described. Minimal changes in the crystalline structure of FOD occurred after five cycles at pH 7 (Hu et al. 2019) and pH 4 (Li et al. 2018). Nevertheless, the commercial FOD catalyst used in this study changed from yellow to orange color during the photo-Fenton treatment in the PYR degradation at pH 6. The Raman spectrum of the catalyst before and after the first cycle of use (dried to 80 °C) showed differences in the main peak (Fig. 4). The unused FOD catalyst showed the bands coincide with C-O bond (1468 and 1432 cm^{-1}), C-C (913 cm^{-1}), δ-ring (519, 584 cm^{-1}), Fe-O (204, 244 cm^{-1}), and FeO_2 (117 cm^{-1}) assigned to the vibrational modes of FOD structure (Edwards and Russell 1998; D'Antonio et al. 2009), whereas the spectrum of the used catalyst showed other bands (A_{1g} 222, 490, E_g 290, 408, 607 cm^{-1}) that coincide with the characteristic vibrational modes of hematite (Fe_2O_3), according to Das and Hendry (2011). This change was ascribed to the photolysis of oxalate and the oxidation of Fe^{2+} to Fe^{3+}. Liu et al. (2017) also reported low stability of iron oxalate after the first use that was attributed to iron leaching.

3.3 Fe^{2+}/Ox Molar Ratio Effect

Another iron source recently used in photo-Fenton is the in situ formation of the iron oxalate complex. Different Fe^{2+}/Ox molar ratios (1:3, 1:6, and 1:9) were tested to evaluate the effect of oxalate ion. In this work, complexes with 0.1 mmol L^{-1} $FeSO_4$ and the adequate

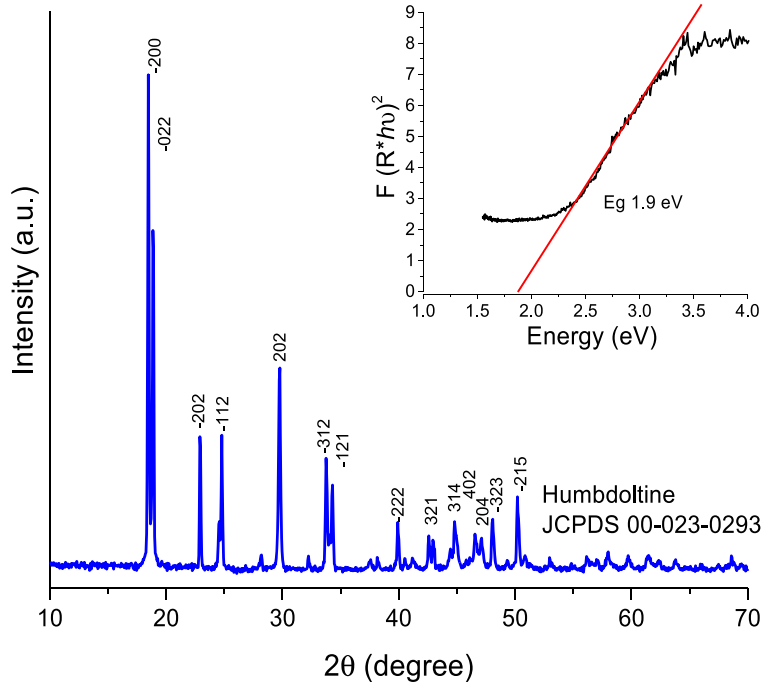

Fig. 2 Diffraction pattern and Kubelka-Munk graph (insert) of FOD

amount of oxalate were in situ prepared. The 1:20 molar ratio Fe^{2+}/H_2O_2 was selected from our previously described results (Fig. 1). In Fig. 5, a positive effect on PYR degradation was observed with Fe^{2+}/Ox 1:3, reaching a higher PYR degradation rate within the first minutes of reaction compared to the conventional photo-Fenton treatment (i.e., using $FeSO_4$) for all pH values. The complete degradation was achieved in only 15 min at pH 3. These results could be attributed to a higher quantum yield of $Fe(C_2O_4)_3^{3-}$ compared with that of $Fe(OH)_2^+$ or $Fe(OH)^{2+}$ for Fe^{2+} regeneration (Dias et al. 2014; Souza et al. 2014). Besides, a significant positive contribution of Fe^{2+}/Ox was observed using molar ratio 1:3 at pH 6 reaching a degradation

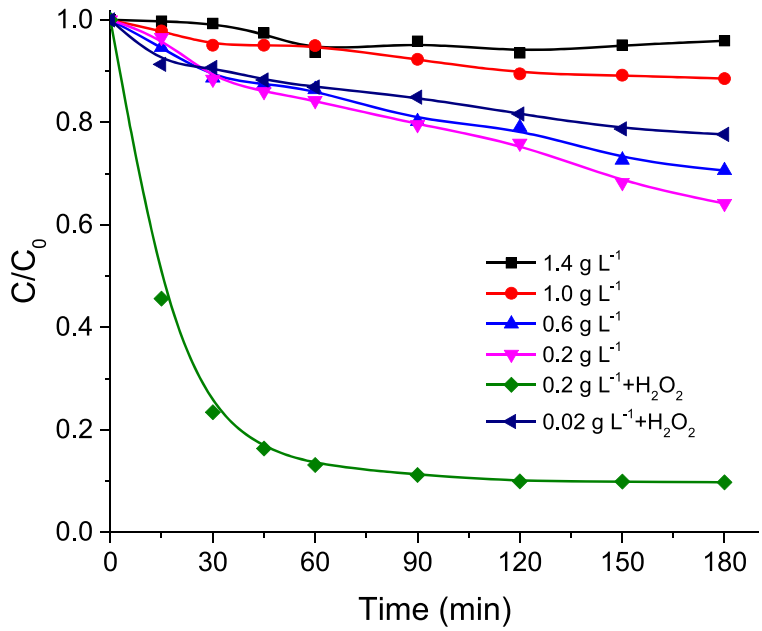

Fig. 3 Pyrazinamide degradation at pH 6 using different catalyst loading of FOD with and without H_2O_2

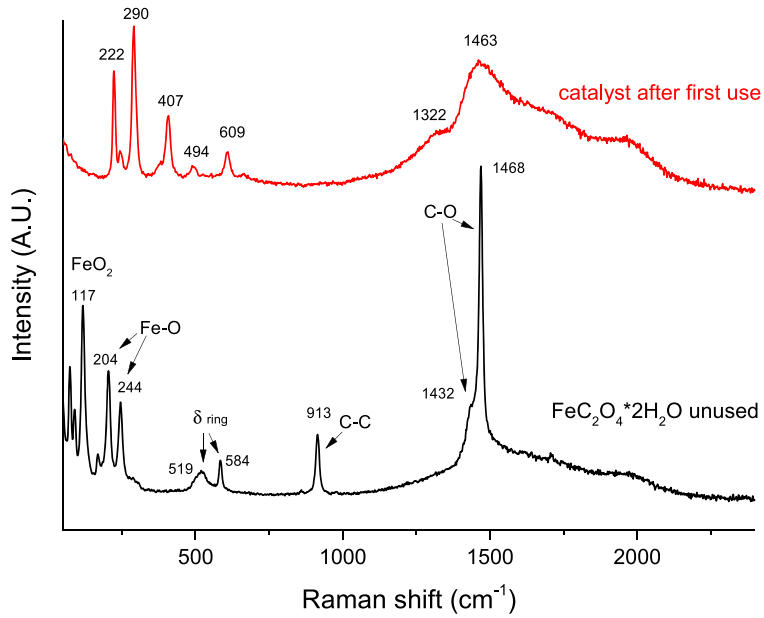

Fig. 4 Raman spectra of ferrous oxalate before and after use in the photo-Fenton treatment

rate of 9.36×10^{-2} min^{-1} compared to that using $FeSO_4$ at the same experimental conditions (1.61×10^{-2} min^{-1}) (Table 1); which is in agreement with a previous study (Expósito et al. 2018) that reports almost complete degradation of carbamazepine at pH 5 using Fe^{2+}/Ox molar ratio 1:3 under solar radiation.

Although a superior result was obtained with Fe^{2+}/Ox 1:3 molar ratio than $FeSO_4$ or FOD, degradation percentage of PYR was the maximum after 15 min of reaction at all pH values (Fig. 5). On the contrary, the complete degradation of this antibiotic was achieved using $FeSO_4$ in 180 min (Fig. 1). To better understand this behavior, the concentrations of Fe^{2+}, Fe^{3+}, and H_2O_2 were monitored during the photo-Fenton process using $FeSO_4$ at pH 3 (Fig. 6a) and Fe^{2+}/Ox 1:3 (Fig. 6b) as iron sources. Fast oxidation of Fe^{2+} was observed when $FeSO_4$ acts as a catalyst, producing an instantaneous color change of the solution from colorless to

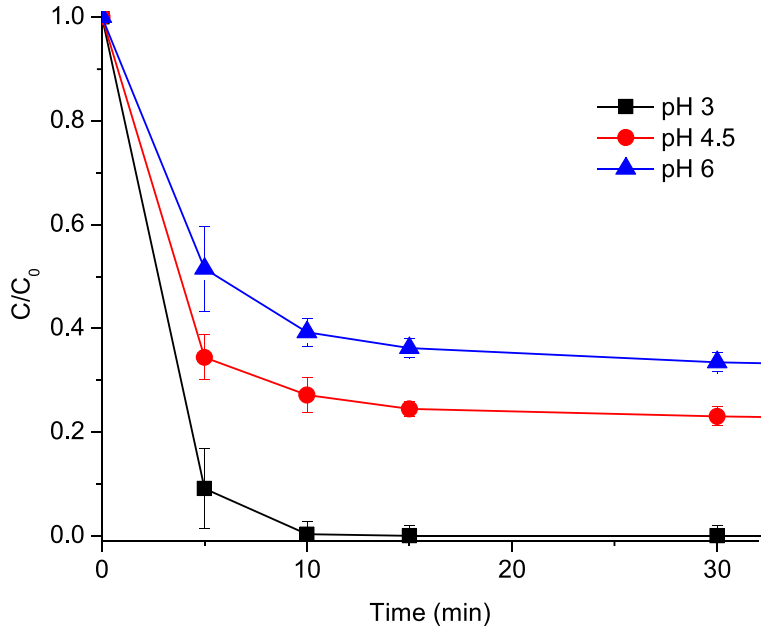

Fig. 5 Pyrazinamide degradation by the photo-Fenton process at different pH values (■) 3, (●) 4.5, (▲) 6, using Fe^{2+}/Ox (1:3). $n = 2$

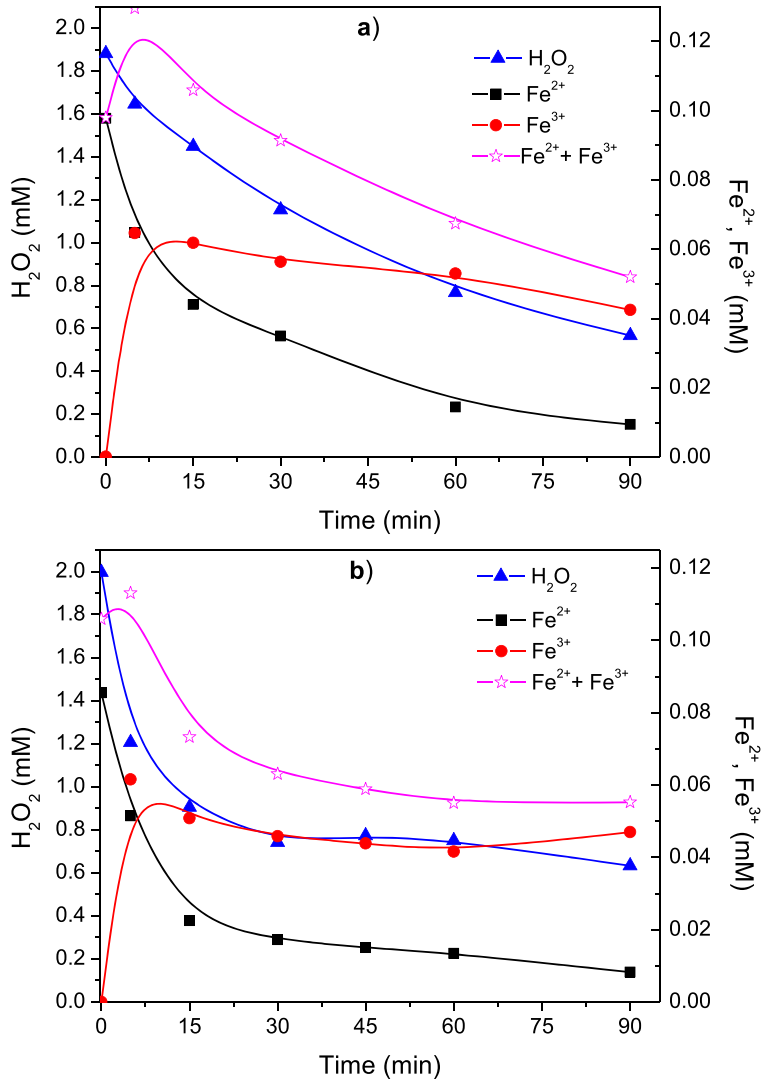

Fig. 6 Evolution of (●) Fe^{2+}, (▲) Fe^{3+}, and (■) H_2O_2 during PYR degradation in 1:20 Fe^{2+}/H_2O_2 molar ratio at pH 3 using (a) $FeSO_4$,and (b) Fe/Ox (1:3). $n = 2$

yellowish caused by Fe^{3+} production, reaching a plateau in concentration after 15 min of reaction, whereas H_2O_2 was slowly consumed. This result could be explained by the complete degradation of PYR using $FeSO_4$ after 180 min. On the other hand, the faster consumption of Fe^{2+} and H_2O_2 observed using Fe^{2+}/Ox 1:3, in the first 15 min (Fig. 6b), is following the highest degradation rate of the pollutant, and the reason why the reaction stops after 15 min (Fig. 3 and Table 1).

It is worth to mention that the total iron amount (Fe^{2+} plus Fe^{3+}) quantified during the reaction in both cases was lower than the initial quantity. This effect can be adscribed to the formation of iron-pyrazine ring complexes with the unpaired electrons of nitrogen in the molecule (Pannu et al. 2012; Shirvan and Haydari Dezfuli 2012) as was previously described for other antibiotics with nitrogen heterocycle (Dias et al. 2014). These complexes could lead to a decrease in degradation rate using $FeSO_4$, while by using Fe^{2+}/Ox 1:3, these iron-pyrazine ring complexes could be inhibited, causing a higher degradation rate and faster H_2O_2 and iron consumption as is observed in Fig. 6b in the first 15 min of reaction. Elevated consumption of H_2O_2 in the presence of oxalate compared to conventional photo-Fenton was also described in a previous study (Souza et al. 2014). Moreover, the presence of oxalate could increase the degradation rate of PYR through Eqs. 8 and 9, causing a fast iron release to the bulk solution.

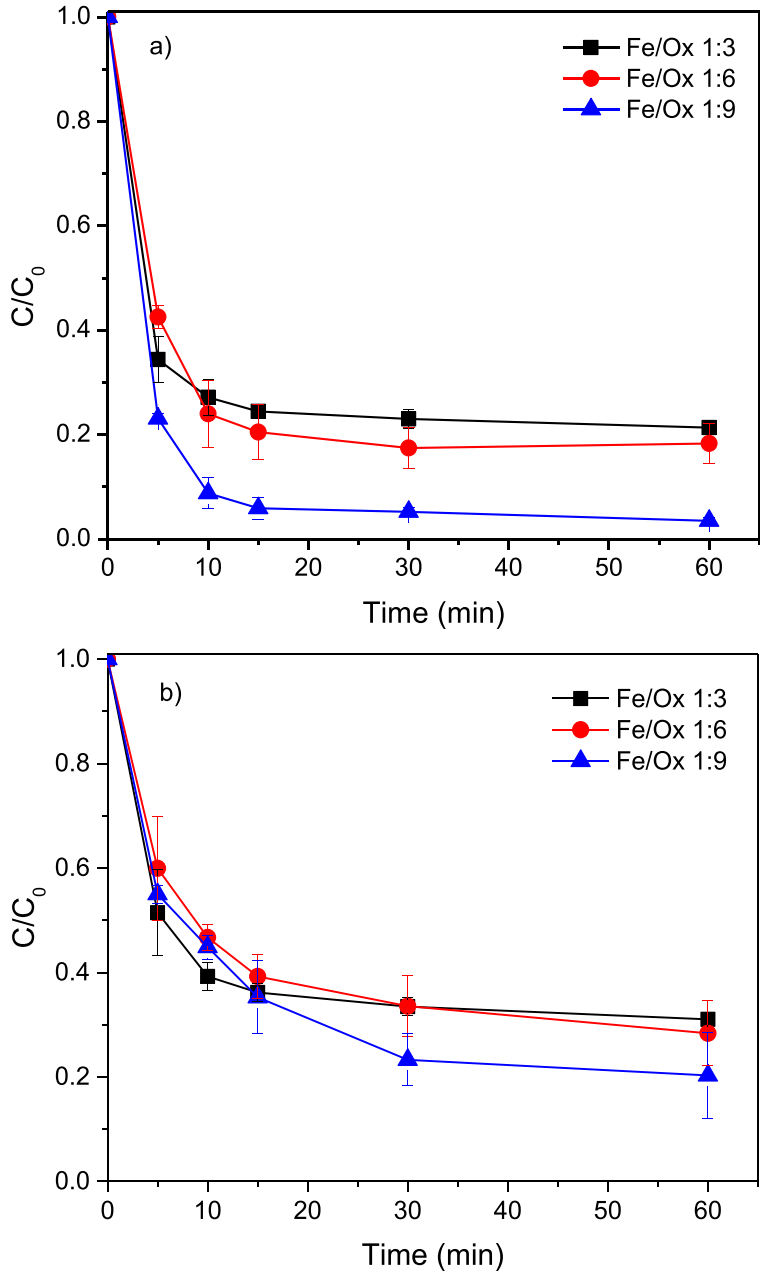

Fig. 7 Pyazinamide degradation by the photo-Fenton process at pH (a) 4.5 and (b) 6, using different iron Fe^{2+}/Ox molar ratio: (■) 1:3, (●) 1:6, and (▲) 1:9. $n = 2$

Regarding Fe^{2+}/Ox molar ratio, it has stated that an excess of the ligand could act as HO• scavenger (Xiao et al. 2014). However, better results were reported using elevated oxalate amounts, avoiding iron precipitation since the fast ferrioxalate photo-decarboxylation occurs under UV radiation (De Luca et al. 2014; Dias et al. 2014; Conte et al. 2016). Thus, the PYR degradation efficiency was also evaluated using Fe^{2+}/Ox molar ratio 1:6 and 1:9 at pH > 3. Small differences between Fe^{2+}/Ox 1:3 and 1:6 were observed at pH 4.5 and 6 (Fig. 7a and b); however, the degradation percentage was enhanced as the $Fe2^{+}$/Ox molar ratio increase to 1:9 up to 96.5 and 79.6% in 60 min at pH 4.5 and 6, respectively. On the other hand, iron precipitation was evident after 15 min of reaction at pH 6, which explains the lower degradation efficiency. Better degradation efficiencies have been described when the Fe^{2+}/Ox molar ratio increases from 1:3 to 1:10 at pH 4.5–6 (Soares et al. 2015) or from 1:3 to 1:9 at pH 6

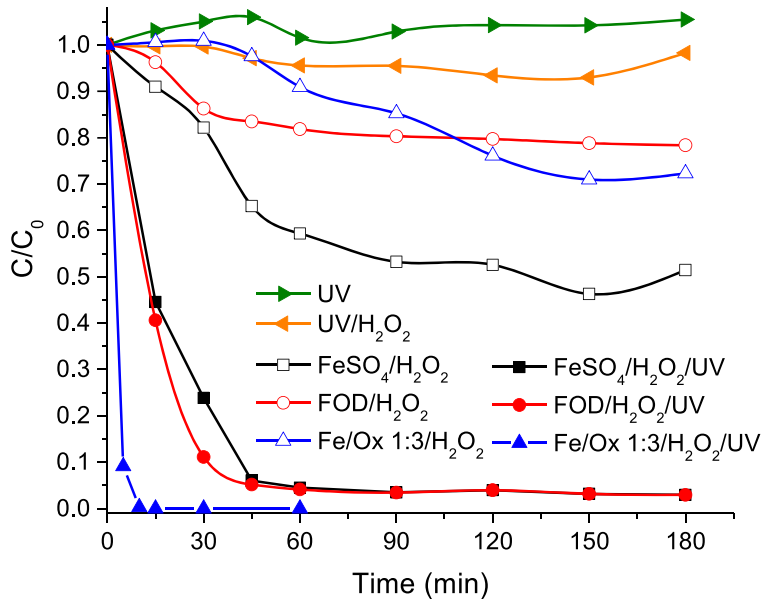

Fig. 8 Control test and comparison of the oxidative processes in the degradation of pyrazinamide at pH 3 using different iron sources. (►) UV photolysis, (◄) UV/H_2O_2. Dark (empty symbols) and photo (filled symbols) Fenton assays using (□, ■) $FeSO_4$, (○, ●) FOD and (Δ, ▲) Fe^{2+}/Ox (1:3)

(Souza et al. 2014). In contrast, Nogueira et al. (2017) described that the degradation of levofloxacin was slightly improved at pH 5, with the increase of the oxalate amount (Nogueira et al. 2017); however, they also monitored oxalate concentration, and it was almost consumed in the first stage of the reaction. These results confirmed the positive effect of complex formation to enhance the decomposition of contaminants due to an increase in the solubility of iron and the photosensitivity of the complex (Nogueira et al. 2017; Expósito et al. 2018).

3.4 Iron Sources Comparison

Figure 8 shows PYR degradation at pH 3 comparing different iron sources, where the highest degradation rate was observed with Fe^{2+}/Ox 1:3, while similar results with $FeSO_4$ and FOD (Fe^{2+}/H_2O_2 1: 20) were obtained. Also, from Table 1, it can be seen comparable degradation rates using $FeSO_4$ and FOD at pH 3 and 4.5; however, the slightly higher k_{app} at pH 3 and 4.5 were observed using FOD than that using $FeSO_4$ (Table 1) since $C_2O_4^{2-}$ could also participate in PYR

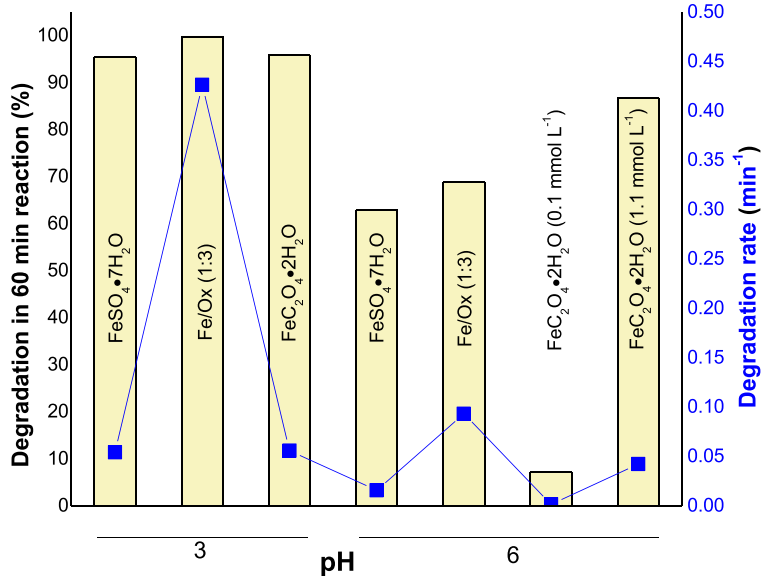

Fig. 9 Comparison of the oxidative processes in the degradation of pyrazinamide using different iron sources ($FeSO_4$, FOD, and Fe^{2+}/Ox (1:3)) at pH 3 and 6

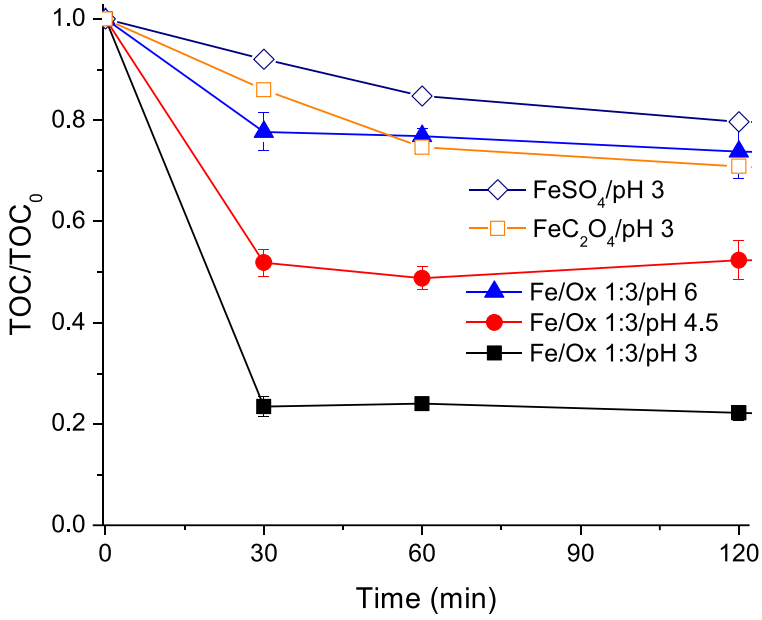

Fig. 10 TOC removal in the photo-Fenton degradation of PYR using $[Fe^{2+}] = 0.1$ mmol L^{-1}, $[H_2O_2] = 2$ mmol L^{-1}. Comparison between different iron sources: (◊) $FeSO_4$, and (□) FOD at pH 3, and Fe^{2+}/Ox 1:3 at pH (■) 3, (●) 4.5, and (▲) 6. $n = 2$

degradation through the formation of reactive species (Eq. 8). As it is well known, the Fenton reaction reaches the highest efficiency at pH 3; however, it is worth to mention that PYR was completely degraded at near-neutral pH (i.e., pH 6) by the photo-Fenton process using Fe^{2+}/Ox (1:3) or using FOD (0.2 g L^{-1}, 1.1 mmol L^{-1}) (Fig. 9). At pH 6, the highest degradation rate was achieved with Fe^{2+}/Ox (1:3), but the degradation percentage was lower than those obtained with FOD, because using Fe^{2+}/Ox (1:3), degradation stops after 15 min. Some authors have reported stability during the reuse of FOD, which could be another advantage of the FOD use (Li et al. 2018; Hu et al. 2019).

As control tests, individual oxidative processes were carried out at pH 3 and Fe^{2+}/H_2O_2 1:20 (Fig. 8). It was demonstrated that neither UV radiation (365 nm) nor UV/H_2O_2 system allowed PYR degradation due to the high stability of this molecule. On the other hand, by the Fenton process, PYR was partially oxidized, reaching 48.5, 21.6, and 20.7% of degradation in 180 min using $FeSO_4$, FOD, and Fe^{2+}/Ox (1:3), respectively. The lower percentage achieved in the presence of oxalate could be attributed to the small amount of available Fe^{2+} in solution to react with H_2O_2. These results were in agreement with previous works where Fe^{2+} regeneration from iron complexes was limited in the absence of UV radiation compared to the result in the irradiated system (Souza et al. 2014; Clarizia et al. 2017). In contrast, the photo-Fenton process using $FeSO_4$, FOD, and Fe^{2+}/Ox (1:3) allowed complete degradation of PYR attributed to a synergistic effect that involves the generation of $HO^{\bullet}$ radicals through Fenton reaction, Fe^{2+} regeneration, and H_2O_2 photolysis (Eqs. 1, 3, and 4, respectively).

The higher efficiency achieved with Fe^{2+}/Ox (1:3) than that using FOD could be explained by oxalate participation (Eqs. 7 and 8), where Fe^{3+} formed in the Fenton reaction is reduced to Fe^{2+} promoting $C_2O_4^{\bullet-}$ generation, that in the presence of oxygen allows the formation of $O_2^{\bullet-}$ (Clarizia et al. 2017), which also could oxidize the organic contaminant. The efficiency of ferroxioxalate to degrade contaminants was also described in the absence of H_2O_2 (Jeong and Yoon 2004; Chen et al. 2020), even under dark conditions (Lee et al. 2014).

On the other hand, it is difficult to estimate and compare the mineralization performance of the conventional photo-Fenton with that achieved using different iron sources since oxalate has an organic contribution on the reaction; however, it has been described that oxalate is easily photolyzed under UV light (Xiao et al. 2014; Nogueira et al. 2017). In this work, TOC percentages were 20.3, 29.1, and 79.5% at pH 3 in 120 min using $FeSO_4/H_2O_2$ (1:20), FOD, and Fe^{2+}/Ox (1:3), respectively (Fig. 10). Some authors compared mineralization rate using Fe^{2+}/Ox complex and the conventional iron source, obtaining better results with Fe^{2+}/Ox ~ 1:3 at pH 3 (Monteagudo et al. 2013) and even at pH 5 (Souza

et al. 2014). This behavior could be due to an increase in Fe solubilization and photosensitivity of the complexes regenerating Fe^{2+}.

In Fig. 10, TOC abatement was also compared using Fe^{2+}/Ox 1:3 at pH 4.5 and 6, obtaining 48.0 and 27.0% of mineralization in 30 min, respectively. However, the mineralization stopped after the first 15 min of reaction, in agreement with the degradation behavior (Fig. 7). The high mineralization degree with Fe^{2+}/Ox 1:3 was ascribed to both PYR and oxalate elimination. Although oxalate could contribute to the organic matter in the effluent, some authors consider that the complete mineralization of oxalate is unnecessary, since iron precipitation could be accelerated, reducing the degradation efficiency (Conte et al. 2016).

The incomplete mineralization of PYR (63% in 300 min) also was reported using TiO_2 mediated heterogeneous photocatalysis under UV light (Guevara-Almaraz et al. 2015). On the contrary, 97% of mineralization (measured as chemical oxygen demand) was described by electro-Fenton within 7 h (Arhoutane et al. 2019). The partial mineralization reached was attributed to the high stability of pyrazine ring, which is a recalcitrant moiety due to the two nitrogen atoms in para-position (Jing et al. 2011; Kaur and Pal 2013).

4 Conclusions

The photo-Fenton process is an effective treatment for PYR degradation using Fe^{2+}/H_2O_2 molar ratio of 1:20 and different iron sources such as $FeSO_4$, FOD, and Fe^{2+}/Ox 1:3, reaching > 95% degradation at pH 3 and more than 86% at pH 6 in 60 min. Elevated H_2O_2 amount acts as $HO^{\bullet}$ scavenger and shows a negative effect mainly using the FOD source. The complete PYR degradation was achieved only with $FeSO_4$ at pH 6 after 180 min with a k_{app} 1.61×10^{-2} min^{-1}; however, the degradation rate was higher with Fe^{2+}/Ox 1:3 (9.36×10^{-2} min^{-1}), which demonstrated the beneficial effect of oxalate in PYR degradation by the photo-Fenton process. FOD also is a promising catalyst in the photo-Fenton reaction at pH 6 using the adequate catalyst loading (0.2 g L^{-1}). The comparison of the oxidative processes on PYR degradation showed the following trend: photo-Fenton > Fenton > H_2O_2/UV ≈ photolysis ascribed to the synergistic effect caused by the Fenton reaction, ferrous ion photo-regeneration, H_2O_2 photolysis, and oxalate participation. The accomplished partial mineralization could be attributed to pyrazine ring stability and the formation of complexes with iron in the reaction medium.

Acknowledgments The authors acknowledge financial support from Facultad de Ciencias Químicas of the Universidad Autónoma de Nuevo León. We also thank F. Espiricueta Candelaria for the technical support in HPLC analysis.

Compliance with Ethical Standards

Conflict of Interest The authors declare that they have no conflict of interest.

References

Alalm, M. G., Tawfik, A., & Ookawara, S. (2015). Degradation of four pharmaceuticals by solar photo-Fenton process: kinetics and costs estimation. *Journal of Environmental Chemical Engineering, 3*, 46–51.

Arhoutane, M. R., Yahya, M. S., Karbane, M. E., Guessous, A., Chakchak, H., & El Kacemi, K. (2019). Removal of pyrazinamide and its by-products from water: treatment by electro-Fenton process and feasibility of a biological post-treatment. *Mediterranean Journal of Chemistry, 8*(1), 53–65.

Chen, Y., Xi, X., Yu, G., Cao, Q., Wang, B., VINCE, F., & Hong, Y. (2015). Pharmaceutical compounds in aquatic environment in China: locally screening and environmental risk assessment. *Frontiers of Environmental Science & Engineering, 9*(3), 394–401.

Chen, N., Wan, Y., Zhan, G., Wang, X., Li, M., Zhang, L. (2020) Simulated solar light driven roxarsone degradation and arsenic immobilization with hematite and oxalate. *Chemical Engineering Journal.* In press, https://doi.org/10.1016/j.cej.2019.123254.

Clarizia, L., Russo, D., Di Somma, I., Marotta, R., & Andreozzi, R. (2017). Homogeneous photo-Fenton processes at near neutral pH: a review. *Applied Catalysis B: Environmental, 209*, 358–371.

Conte, L. O., Schenone, A. V., & Alfano, O. M. (2016). Photo-Fenton degradation of the herbicide 2,4-in aqueous medium at pH conditions close to neutrality. *Journal of Environmental Management, 170*, 60–69.

D'Antonio, M. C., Wladimirsky, A., Palacios, D., Coggiola, L., González-Baró, A. C., & Baran, E. J. (2009). Spectroscopic investigations of iron(II) and iron(III) oxalates. *Journal of the Brazilian Chemical Society, 20*(3), 445–450.

Das, S., & Hendry, M. J. (2011). Application of Raman spectroscopy to identify iron minerals commonly found in mine wastes. *Chemical Geology, 290*(3–4), 101–108.

De Lima Perini, J. A., Perez-Moya, M., & Nogueira, R. F. P. (2013). Photo-Fenton degradation kinetics of low

ciprofloxacin concentration using different iron sources and pH. *Journal of Photochemistry and Photobiology A: Chemistry, 259*, 53–58.

De Luca, A., Dantas, R. F., & Esplugas, S. (2014). Assessment of iron chelates efficiency for photo-Fenton at neutral pH. *Water Research, 61*, 232–242.

Dias, I. N., Souza, B. S., Pereira, J. H. O. S., Moreira, F. C., Dezotti, M., Boaventura, R. A. R., & Vilar, V. J. P. (2014). Enhancement of the photo-Fenton reaction at near neutral pH through the use of ferrioxalate complexes: a case study on trimethoprim and sulfamethoxazole antibiotics removal from aqueous solutions. *Chemical Engineering Journal, 247*, 302–313.

Edwards, H. G. M., & Russell, N. C. (1998). Vibrational spectroscopic study of iron(II) and iron(III) oxalates. *Journal of Molecular Structure, 443*(1–3), 223–231.

Eisenberg, G. M. (1943). Colorimetric determination of hydrogen peroxide. *Industrial and Engiinering Chemistry, 15*(5), 327–328.

Expósito, A. J., Monteagudo, J. M., Durán, A., San Martín, I., & González, L. (2018). Study of the intensification of solar photo-Fenton degradation of carbamazepine with ferrioxalate complexes and ultrasound. *Journal of Hazardous Materials, 342*, 597–605.

Fan, X., Zhang, L., Li, M., Wang, M., Zhou, X., Cheng, R., et al. (2016). α-Ferrous oxalate dihydrate: a simple coordination polymer featuring photocatalytic and photo-initiated Fenton oxidations. *Science China Materials, 59*(7), 574–580.

Guevara-Almaraz, E., Hinojosa-Reyes, L., Caballero-Quintero, A., Ruiz-Ruiz, E., Hernández-Ramírez, A., & Guzmán-Mar, J. L. (2015). Potential of multisyringe chromatography for the on-line monitoring of the photocatalytic degradation of antituberculosis drugs in aqueous solution. *Chemosphere, 121*, 68–75.

Hu, L., Wang, P., Xiong, S., Chen, S., Yin, X., Wang, L., & Wang, H. (2019). The attractive efficiency contributed by the in-situ reactivation of ferrous oxalate in heterogeneous Fenton process. *Applied Surface Science, 467–468*, 185–192.

Jeong, J., & Yoon, J. (2004). Dual roles of CO2− for degrading synthetic organic chemicals in the photo/ferrioxalate system. *Water Research*, 38(16), 3531–3540.

Jing, J., Liu, M., Colvin, V. L., Li, W., & Yu, W. W. (2011). Photocatalytic degradation of nitrogen-containing organic compounds over TiO_2. *Journal of Molecular Catalysis A: Chemical, 351*, 17–28.

Jo, W. K., & Natarajan, T. S. (2015). Influence of TiO_2 morphology on the photocatalytic efficiency of direct Z-scheme g-C_3N_4/TiO_2 photocatalysts for isoniazid degradation. *Chemical Engineering Journal, 281*, 549–565.

Jung, E., & Baek, K. (2019). Selective recovery of ferrous oxalate and removal of arsenic and other metals from soil-washing wastewater using a reduction reaction. *Journal of Cleaner Production, 221*, 635–643.

Kaur, J., & Pal, B. (2013). Photocatalytic degradation of N-heterocyclic aromatics-effects of number and position of nitrogen atoms in the ring. *Environmental Science and Pollution Research, 20*(6), 3956–3964.

Kwan, C. Y., & Chu, W. (2007). The role of organic ligands in ferrous-induced photochemical degradation of 2,4-dichlorophenoxyacetic acid. *Chemosphere, 67*(8), 1601–1611.

Lee, J., Kim, J., & Choi, W. (2014). Oxidation of aquatic pollutants by ferrous-oxalate complexes under dark aerobic conditions. *Journal of Hazardous Materials, 274*, 79–86.

Li, K., Liang, Y., Yang, J., Yang, G., & Xie, X. (2018). α-Ferrous oxalate dihydrate: an Fe-based one-dimensional metal organic framework with extraordinary photocatalytic and Fenton activities. *Catalysis Science & Technology, 8*, 6057–6061.

Liu, Z. J., Liu, W., Wang, Y., & Guo, M. L. (2016, 178). Preparation of β-ferrous oxalate dihydrate layered nanosheets by mechanochemical method and its visible-light-driven photocatalytic performance. *Materials Letters, 83*, –86.

Liu, Y., et al. (2017). $NiFe(C_2O_4)_x$ as a heterogeneous Fenton catalyst for removal of methyl orange. *Journal of Environmental Management, 192*, 150–155.

Liu, F., Peng, C., Wilson, B. P., & Lundström, M. (2019). Oxalic acid recovery from high iron oxalate waste solution by a combination of ultrasound-assisted conversion and cooling crystallization. *ACS Sustainable Chemistry & Engineering, 7*, 17372–17378.

Luo, Y., Guo, W., Ngo, H. H., Nghiem, L. D., Hai, F. I., Zhang, J., et al. (2014). A review on the occurrence of micropollutants in the aquatic environment and their fate and removal during wastewater treatment. *Science of the Total Environment, 473–474*, 619–641.

Magwira, C. A., Aneck-Hahn, N., & Taylor, M. B. (2019). Fate, occurrence and potential adverse effects of antimicrobials used for treatment of tuberculosis in the aquatic environment in South Africa. *Environmental Pollution, 254*, 112990.

Manenti, D. R., Soares, P. A., Módenes, A. N., Espinoza-Quiñones, F. R., Boaventura, R. A. R., Bergamasco, R., et al. (2015). Insights into solar photo-Fenton process using iron(III)-organic ligand complexes applied to real textile wastewater treatment. *Chemical Engineering Journal, 266*, 203–212.

Monteagudo, J. M., Durán, A., Culebradas, R., San Martín, I., & Carnicer, A. (2013). Optimization of pharmaceutical wastewater treatment bysolar/ferrioxalate photocatalysis. *Journal of Environmental Management, 128*, 210–219.

Muñoz del Carpio-Toia, A., Sánchez-Pérez, H. J., Verges de López, C., López-Dávila, L. M., Sotomayor-Saavedra, M. A., & Sorokin, P. (2018). Tuberculosis en América Latina y el Caribe: reflexiones desde la bioética. *Persona y bioética, 22*(2), 331–357.

Nogueira, A. A., Souza, B. M., Dezotti, M. W. C., Boaventura, R. A. R., & Vilar, V. J. P. (2017). Ferrioxalate complexes as strategy to drive a photo-Fenton reaction at mild pH conditions: a case study on levofloxacin oxidation. *Journal of Photochemistry and Photobiology A: Chemistry, 345*, 109–123.

Pannu, A. P. S., Lee, S., & Lee, Y. (2012). Diaquabis(pyrazine-2-carboxamide-$\kappa^2 N^1,O$) cobalt(II) dinitrate. *Acta Crystallographica Section E Structure Reports Online, 68*(4), m512–m513.

Pehkonen, S. (1995). Determination of the oxidation states of iron in natural waters. A review. *Analyst, 120*, 2655–2663.

Pereira, J. H. O. S., Queirós, D. B., Reis, A. C., Nunes, O. C., Borges, M. T., Boaventura, R. A. R., et al. (2014). Process enhancement at near neutral pH of a homogeneous photo-Fenton reaction using ferricarboxylate complexes:

application to oxytetracycline degradation. *Chemical Engineering Journal, 253*, 217–228.

Pouran, S. R., Aziz, A., & Wan Daud, W. M. A. (2015). Review on the main advances in photo-Fenton oxidation system for recalcitrant wastewaters. *Journal of Industrial and Engineering Chemistry, 21*, 53–69.

Seiberta, S., Diela, T., Welterc, J. B., de Souza, A. L., Módenes, A. N., Espinoza-Quiñones, F. R., & Borba, F. H. (2017). Performance of photo-Fenton process mediated by Fe (III)-carboxylate complexes applied to degradation of landfill leachate. *Journal of Environmental Chemical Engineering, 5*, 4462–4470.

Shirvan, S., & Haydari Dezfuli, S. (2012). Diaquabis(nitrato-κ ^{2} *O* , *O* ′)bis(pyrazine-2-carboxamide-κ *N* ^{4})cadmium–pyrazine-2-carboxamide (1/2). *Acta Crystallographica Section E Structure Reports Online, 68*(7), m1008–m1009.

Soares, P. A., Batalha, M., Souza, S. M. A., Boaventura, R. A. R., & Vilar, V. J. P. (2015). Enhancement of a solar photo-Fenton reaction with ferric-organic ligands for the treatment of acrylic-textile dyeing wastewater. *Journal of Environmental Management, 152*, 120–131.

Souza, B. S., Moreira, F. C., Dezotti, M., Boaventura, R. A. R., & Vilar, V. J. P. (2014). Intensification of a solar photo-Fenton reaction at near neutral pH with ferrioxalate complexes: a case study on diclofenac removal from aqueous solutions. *Chemical Engineering Journal, 256*, 448–457.

Stets, S., do Amaral, B., Schneider, J. T., de Barros, I. R., de Liz, M. V., Rocha, R., Nagata, N., & Peralta-Zamora, P. (2018). Antituberculosis drugs degradation by UV-based advanced oxidation processes. *Journal of Photochemistry and Photobiology A: Chemistry, 353*, 26–33.

Taheran, M., Naghdi, M., Brar, S. K., Verma, M., & Surampalli, R. Y. (2018). Emerging contaminants: here today, there tomorrow! *Environmental Nanotechnology, Monitoring and Management, 10*, 122–126.

Tran, N. H., Reinhard, M., & Gin, K. Y. H. (2018). Occurrence and fate of emerging contaminants in municipal wastewater treatment plants from different geographical regions-a review. *Water Research, 133*, 182–207.

Villegas-Guzman, P., Giannakis, S., Torres-Palma, R. A., & Pulgarin, C. (2017). Remarkable enhancement of bacterial inactivation in wastewater through promotion of solar photo-Fenton at near-neutral pH by natural organic acids. *Applied Catalysis B: Environmental, 205*, 219–227.

Wang, G., Zhou, A., & Xu, Q. (2019). α-Ferrous oxalate with di ff erent micro scale: synthesis and catalytic degradation e ff ect to rhodamine B*., 91*, 54–60.

Xiao, D., Guo, Y., Lou, X., Fang, C., Wang, Z., & Liu, J. (2014). Distinct effects of oxalate versus malonate on the iron redox chemistry: implications for the photo-Fenton reaction. *Chemosphere, 103*, 354–358.